

X-RAY SPECTROSCOPY OF THE LOW-MASS X-RAY BINARIES 2S 0918–549 AND 4U 1543–624: EVIDENCE FOR NEON-RICH DEGENERATE DONORS

ADRIENNE M. JUETT AND DEEPTO CHAKRABARTY¹

Department of Physics and Center for Space Research, Massachusetts Institute of Technology, Cambridge, MA 02139;

ajuett, deepto@space.mit.edu

Submitted to the Astrophysical Journal

ABSTRACT

We present high-resolution spectroscopy of the neutron-star/low-mass X-ray binaries 2S 0918–549 and 4U 1543–624 with the High Energy Transmission Grating Spectrometer onboard the *Chandra X-ray Observatory*. Previous low-resolution spectra of both sources showed a broad line-like feature at 0.7 keV that was originally attributed to unresolved line emission. We recently showed that this feature could also be due to excess Ne absorption, and this is confirmed by the new high-resolution *Chandra* spectra. The spectra are each well fit by an absorbed power-law + blackbody model with a modified Ne/O number ratio of 0.7 ± 0.3 for 2S 0918–549 and 1.8 ± 0.4 for 4U 1543–624, compared to the interstellar-medium value of 0.18. We suggest that 2S 0918–549 and 4U 1543–624 are ultracompact binaries with degenerate dwarf companions and that the unusual abundances reflect the companion composition.

Subject headings: binaries: close — stars: neutron — stars: individual (2S 0918–549) — stars: individual (4U 1543–624) — X-rays: binaries

1. INTRODUCTION

Low mass X-ray binaries (LMXBs) consist of a neutron star (NS) or black hole (BH) in orbit with a $\lesssim 1 M_{\odot}$ companion. An intriguing sub-class of LMXBs are the ultracompact binaries that have orbital periods less than 80 minutes. Hydrogen-rich companions cannot sustain a LMXB system with such a short orbital period (Paczynski & Sienkiewicz 1981). However, orbital periods $\lesssim 80$ min are predicted for hydrogen-deficient or degenerate companions (Joss, Avni, & Rappaport 1978; Nelson, Rappaport, & Joss 1986), and this was confirmed with the orbital period measurements of the X-ray pulsar 4U 1626–67 ($P_{\text{orb}}=42$ min; Middleditch et al. 1981), the X-ray dipper 4U 1915–05 ($P_{\text{orb}}=50$ min; White & Swank 1982; Walter et al. 1982), the X-ray bursters 4U 1820–30 ($P_{\text{orb}}=11$ min; Stella, Friedhorsky, & White 1987) and 4U 1850–087 ($P_{\text{orb}}=21$ min; Homer et al. 1996), and the detection of the white dwarf analogs, the AM CVn systems (e.g. Warner 1995). In addition, the two recently discovered millisecond X-ray pulsars XTE J1751–305 and XTE J0929–314 were also found to be ultracompact binaries with $P_{\text{orb}}=42$ and 44 min, respectively (Markwardt & Swank 2002; Galloway et al. 2002). The conventional wisdom has been that the companions in ultracompact LMXBs are the remains of He white dwarfs (WDs) that have transferred a significant fraction of their mass to the NS. However, recent X-ray spectral evidence indicates that some companions may be Ne-rich (Schulz et al. 2001; Juett, Psaltis, & Chakrabarty 2001), which suggests the possibility of C-O or O-Ne-Mg WD companions. The growing population of these exotic ultracompact systems, as well as the new evidence for Ne-rich companions, has interesting implications for the formation and evolution of binary systems. Here we discuss two other NS/LMXBs that may also be ultracompact binaries.

Both 2S 0918–549 ($l = 275.9^\circ$, $b = -3.8^\circ$) and 4U 1543–624 ($l = 321.8^\circ$, $b = -6.3^\circ$) have been observed by all of the major X-ray satellites since *Uhuru*. McClintock et al. (1978) identified the optical counterpart of 4U 1543–624 based on the SAS-

3 position, which was confirmed by *HEAO 1*. The flux measurements of 4U 1543–624 are roughly constant over the last 25 years (Singh, Apparao, & Kraft 1994; Christian & Swank 1997; Asai et al. 2000; Juett et al. 2001) with no periodicities from 50 s – 10,000 s found in the *EXOSAT* data. In contrast, 2S 0918–549 shows a factor of 10 X-ray variability but has no known periodicities in either the X-ray or optical bands down to timescales of 1 hour (Forman et al. 1978; Warwick et al. 1981; Chevalier & Illovaiky 1987; Smale & Lochner 1992; Christian & Swank 1997; Schulz 1999; Jonker et al. 2001). Chevalier & Illovaiky (1987), using the *Einstein* HRI position, identified an ultraviolet-bright optical counterpart for 2S 0918–549 and suggested a source distance of 15 kpc based on the properties of other LMXBs. Recently, Jonker et al. (2001) detected a type I X-ray burst from 2S 0918–549 and derived an upper limit to the distance of 4.9 kpc from radius expansion arguments.

We have identified both 2S 0918–549 and 4U 1543–624 as being part of a class of four NS/LMXBs all having a similar feature at 0.7 keV in their low-resolution spectra (Juett et al. 2001). This feature had been attributed to unresolved line emission from Fe and O (see, e.g., Christian, White, & Swank 1994; White, Kallman, & Angelini 1997). However, a high-resolution observation of the brightest of these sources, 4U 0614+091, with the *Chandra X-Ray Observatory*, failed to detect any emission lines, finding instead an unusually high Ne/O number ratio along the line of sight (Paevels et al. 2001). Previously, we showed that the *ASCA* spectra of all four sources are well fit *without* a 0.7 keV emission line using a model that includes photoelectric absorption due to excess Ne along the lines of sight and presumably local to the sources. We suggested that the systems are ultracompact binaries with Ne-rich degenerate donors (Juett et al. 2001). In this paper, we present the high-resolution *Chandra* spectra of two more of these sources, 2S 0918–549 and 4U 1543–624, which support our earlier explanation.

¹ Alfred P. Sloan Research Fellow

2. OBSERVATIONS AND DATA REDUCTION

Chandra observed 2S 0918–549 on 2000 July 19 and 4U 1543–624 on 2000 September 12 for 30 ks each using the High Energy Transmission Grating Spectrometer (HETGS) and the Advanced CCD Imaging Spectrometer (ACIS; Weisskopf et al. 2002). The HETGS carries two transmission gratings: the Medium Energy Gratings (MEGs) with a range of 2.5–31 Å (0.4–5.0 keV) and the High Energy Gratings (HEGs) with a range of 1.2–15 Å (0.8–10.0 keV). The HETGS spectra are imaged by ACIS, an array of six CCD detectors. The HETGS/ACIS combination provides both an undispersed (zeroth order) image and dispersed spectra from the gratings. The various orders overlap and are sorted using the intrinsic energy resolution of the ACIS CCDs. The first-order MEG (HEG) spectrum has a spectral resolution of $\Delta\lambda = 0.023$ Å (0.012 Å).

The “level 1” event files were processed using the CIAO v2.2 data analysis package². For both sources, the standard CIAO spectral reduction procedure was performed. During our analysis, it was found that the pipeline tool `acis_detect_afterglow` rejects 3–5% of source photons in grating spectra³. Afterglow is the residual charge left from a cosmic-ray event which is released over several frames and can cause a line-like feature in a grating spectrum. The `acis_detect_afterglow` tool flags events that occur at the same chip coordinates in consecutive frames. For bright sources, the tool also rejects a fraction of the source events. Although only a small fraction of the total, the rejection of source photons by this tool is systematic and non-uniform. Since order-sorting of grating spectra provides efficient rejection of background events, the afterglow detection tool is not necessary. Therefore, we reextracted the event file, retaining those events tagged by the `acis_detect_afterglow` tool. No features were found that might be attributable to afterglow events.

For bright sources, pileup can be a problem for CCD detectors (see, e.g., Davis 2001b). Pileup occurs when two or more photons are incident on the same pixel during the 3.2 s readout time of the ACIS detector. When this happens, the instrument reads just one event at an energy comparable to the sum of the original photons energies, thus reducing the detected count rate and modifying the spectral shape. The zeroth order *Chandra* spectra of both 2S 0918–549 and 4U 1543–624 were heavily affected by pileup (pileup fraction > 80%) and were not used in this analysis. In addition, pileup can also affect dispersed spectra. We checked the dispersed spectra of both sources and found that for 2S 0918–549 no pileup occurred; whereas for 4U 1543–624, there were signs of pileup in the first order MEG spectrum. In dispersed spectra, pileup can affect only a limited wavelength range, particularly where the effective area of the instrument is the highest. For 4U 1543–624, pileup occurred in the range 5–12 Å (1–2.5 keV).

The combined MEG + HEG first order dispersed spectrum of 2S 0918–549 has an average count rate of 3.10 ± 0.18 cts s^{−1}. We examined the total count rate, as well as the count rates in three different energy ranges, to check for changes in the spectral state of 2S 0918–549. We found no evidence for any change of state during the *Chandra* observation. For 4U 1543–624, the first order MEG + HEG count rate is 17.2 ± 0.4 cts s^{−1}.

Similarly, no changes of state of 4U 1543–624 were found. To look for periodic modulations of the X-ray flux, we created lightcurves from the combined first order event files after barycentering and randomizing the event arrival times. Randomizing of the event arrival times consists of adding a random quantity uniformly distributed between 0–3.2 s in order to avoid aliasing caused by the readout time. We searched for modulations of the X-ray flux with frequencies between 4×10^{-5} and 5×10^{-2} Hz. We found no evidence for periodic modulation in either source, with a 90%-confidence upper limit of 2% (2S 0918–549) and 1% (4U 1543–624) for the fractional rms amplitude.

Using the CIAO tool `celldetect`, the zeroth order source position for 2S 0918–549 was determined: R.A.=09^h20^m26^s92 and Dec=−55°12'24.6", equinox J2000.0 (1 σ error of 0.5"). The *Chandra* position for 2S 0918–549 is consistent with the *Einstein* HRI position, 5" error radius, used to identify the optical counterpart (Chevalier & Illovaisky 1987). The zeroth order image of 4U 1543–624 was so heavily piled up that no counts were recorded in the center of the point spread function. `Celldetect` was not able to determine an accurate source position, but the CIAO tool `tgdetect`, which runs `celldetect` in conjunction with grating specific filters and sub-tools, was able to position the zeroth order image of 4U 1543–624: R.A.=15^h47^m54^s47 and Dec=−62°34'05.9", equinox J2000.0 (1 σ error of 0.5"). This position is 1.6" west of the optical position given by Bradt & McClintock (1983).

For 2S 0918–549, we used the standard CIAO tools to create detector response files (ARFs; see Davis 2001a) for the MEG and HEG +1 and −1 order spectra. These were combined when the +/− order spectra were added for the MEG and HEG separately. Two groupings were applied to the data: (1) the data were binned to 0.1 Å for low-resolution continuum modeling and (2) the MEG (HEG) data were binned to 0.03 Å (0.015 Å) for high-resolution studies. We also created background files for the MEG and HEG spectra using the standard CIAO tool. Finally, we used the XSPEC v11 data analysis package (Arnaud 1996) to analyze the background-subtracted spectra of 2S 0918–549.

There are known discrepancies in the quantum efficiencies (QEs) of the front-illuminated (FI) CCDs compared to the back-illuminated (BI) CCDs⁴. An initial analysis using the standard QE files revealed that, for 4U 1543–624, the chip differences were identifiable (especially at high wavelengths) and needed to be corrected. Using a correction table provided by H. L. Marshall of the HETGS instrument team, we modified the QE files available in the standard CIAO calibration database and then used them to create ARFs for the spectral analysis of 4U 1543–624. This modification was not required for the 2S 0918–549 data. Since the first order MEG spectrum of 4U 1543–624 was affected by pileup, we did not use the standard reduction and analysis techniques. Instead, we created ARFs for each chip using the CIAO tool `mkgarf` and then combined them to create +1 and −1 order MEG and HEG ARFs using a custom tool developed by J. Davis of the HETGS instrument team. (This tool is similar to the standard CIAO tool but also correctly calculates the fractional exposure at each response bin.) This was done for compatibility with the grating

² <http://asc.harvard.edu/ciao/>

³ See <http://asc.harvard.edu/ciao/threads/acisdetectafterglow/>

⁴ See http://space.mit.edu/ASC/calib/letg_acis/letg_acis_cal.ps.gz

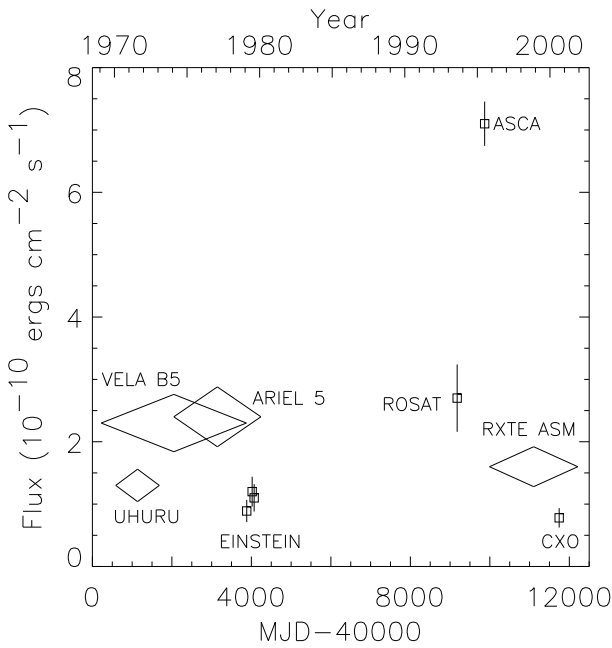


FIG. 1.— The 2–10 keV absorbed flux of 2S 0918–549 in units of 10^{-10} ergs cm^{-2} s^{-1} over the past 30 years. The majority of the observations are reasonably consistent, except for the 1995 ASCA observation, when the source seems to have been in a bright state. The large diamonds represent average flux measurements for monitoring missions, while the small squares represent pointed observations.

pileup kernel available in ISIS⁵, a specialized spectral analysis program for X-ray grating data (Davis 2001b; Houck & DeNicola 2000). The grating pileup kernel, still in development and available only for ISIS, models the effect of pileup on grating spectra, similar to the pileup model available for CCD spectra in ISIS and XSPEC. In order to use the grating pileup kernel, the data and responses were rebinned to 0.033 \AA (0.017 \AA) for the MEG (HEG) to reflect the size of an ACIS event detection cell (3 CCD pixels). We used this binning for the high-resolution spectral study. We also grouped both the MEG and HEG spectra to 0.1 \AA to fit the continuum model. All spectral analysis of 4U 1543–624 was performed using ISIS.

3. SPECTRAL RESULTS

3.1. 2S 0918–549

We fit coarsely binned HEG and MEG spectra jointly with an absorbed power-law + blackbody model. There is no evidence for line emission in the *Chandra* spectra of 2S 0918–549. The best-fit equivalent hydrogen column density is $N_{\text{H}} = (1.8 \pm 0.4) \times 10^{21} \text{ cm}^{-2}$. For comparison, the color excess estimated for the optical counterpart is $E_{B-V} = 0.3 \pm 0.1$ (Chevalier & Illovaisky 1987), consistent with reddening measurements of stars along the line of sight (van Paradijs et al. 1986) and implying $N_{\text{H}} = (1.7 \pm 0.6) \times 10^{21} \text{ cm}^{-2}$, using the empirical relationship between E_{B-V} and N_{H} derived by Predehl & Schmitt (1995).

The absorbed 2–10 keV flux of 2S 0918–549 was 7.8×10^{-11} erg cm^{-2} s^{-1} , which is an order of magnitude lower than the ASCA observation in 1995. The *Chandra* flux measurement is, however, consistent with other past observations, including the

RXTE ASM flux measurements made contemporaneously with the *Chandra* observation (see Figure 1). The spectral shape of the source has been roughly constant over the past 20 years, excluding the addition of a blackbody component in more recent data. The need for the blackbody model is attributable to the greater sensitivity of recent instruments, since the blackbody makes only a modest change in the spectral shape. The ASCA spectral fit gives a photon index $\Gamma = 1.73 \pm 0.02$, while the *Chandra* fit finds a best-fit $\Gamma = 1.92 \pm 0.14$. This difference is not enough to account for the observed change in flux; rather, the source seems to be brighter during the ASCA observation with larger normalizations measured for both the power-law and blackbody components. We suggest that 2S 0918–549 was in a bright state during the ASCA observation, similar to outbursts seen in other LMXBs (e.g., Homan & van der Klis 2000). As seen in X-ray color-color diagrams for sources in outburst, the hard color varies between outburst and quiescent phases while the soft color remains roughly the same (see Muno, Remillard, & Chakrabarty 2002). ASCA and *Chandra* have energy sensitivity which cover only the soft color energy range in standard color-color diagrams, so a spectral difference during an outburst may not be measurable with these instruments.

The residuals from the continuum fit of 2S 0918–549 show evidence for excess Ne absorption at $\approx 0.9 \text{ keV}$. The absorption of Ne and O were each modeled by a multiplicative factor of the form:

$$M(E) = \begin{cases} 1 & \text{for } E < E_{\text{edge}}, \\ \exp[-\tau(E/E_{\text{edge}})^{-3}] & \text{for } E \geq E_{\text{edge}}, \end{cases} \quad (1)$$

with τ and E_{edge} as variable parameters. The more complex Fe-L edge at 0.7 keV (17.5 \AA) was modeled using a table model created from the optical constant measurements by Kortright & Kim (2000), which allowed for both the column density of Fe and the edge energy to vary. The absorption from all other elements was described by the vphabs model. The continuum was again described by a power-law + blackbody. The resulting parameters for the power-law and blackbody models are consistent with the low-resolution fit. We found that to correctly fit the high-wavelength (low-energy) side of the O edge, either a higher N_{H} than found in the low-resolution fit or a non-solar C abundance is required. However, we note that ACIS/LETGS (Low Energy Transmission Grating Spectrometer) spectra of various sources have shown a large ($\tau > 0.5$) and variable instrumental C edge contribution⁶ (H. L. Marshall, private communication) that is not measured in HRC/LETGS spectra and is therefore attributed to the ACIS detector. Since this absorption will also affect the high-wavelength end of the ACIS/HETGS spectra presented here, we chose to allow for a variable C abundance to account for instrumental absorption, while fixing the N_{H} to the best-fit value of the coarsely binned spectrum. The choice of N_{H} is somewhat arbitrary considering that we are fitting separately for the largest contributions to the absorption in the X-ray band (from C and O). We consider our choice of N_{H} reasonable given the consistency of the X-ray and optical N_{H} determinations. The results of the fit can be found in Table 1 and are shown in Figure 2.

From the absorption edge depths, the absorbing column densities of O, Fe, and Ne can be determined along with the equivalent hydrogen column for each element assuming interstellar

⁵ <http://space.mit.edu/CXC/ISIS/>

⁶ See also http://space.mit.edu/CXC/calib/letg_acis/ck_cal.html

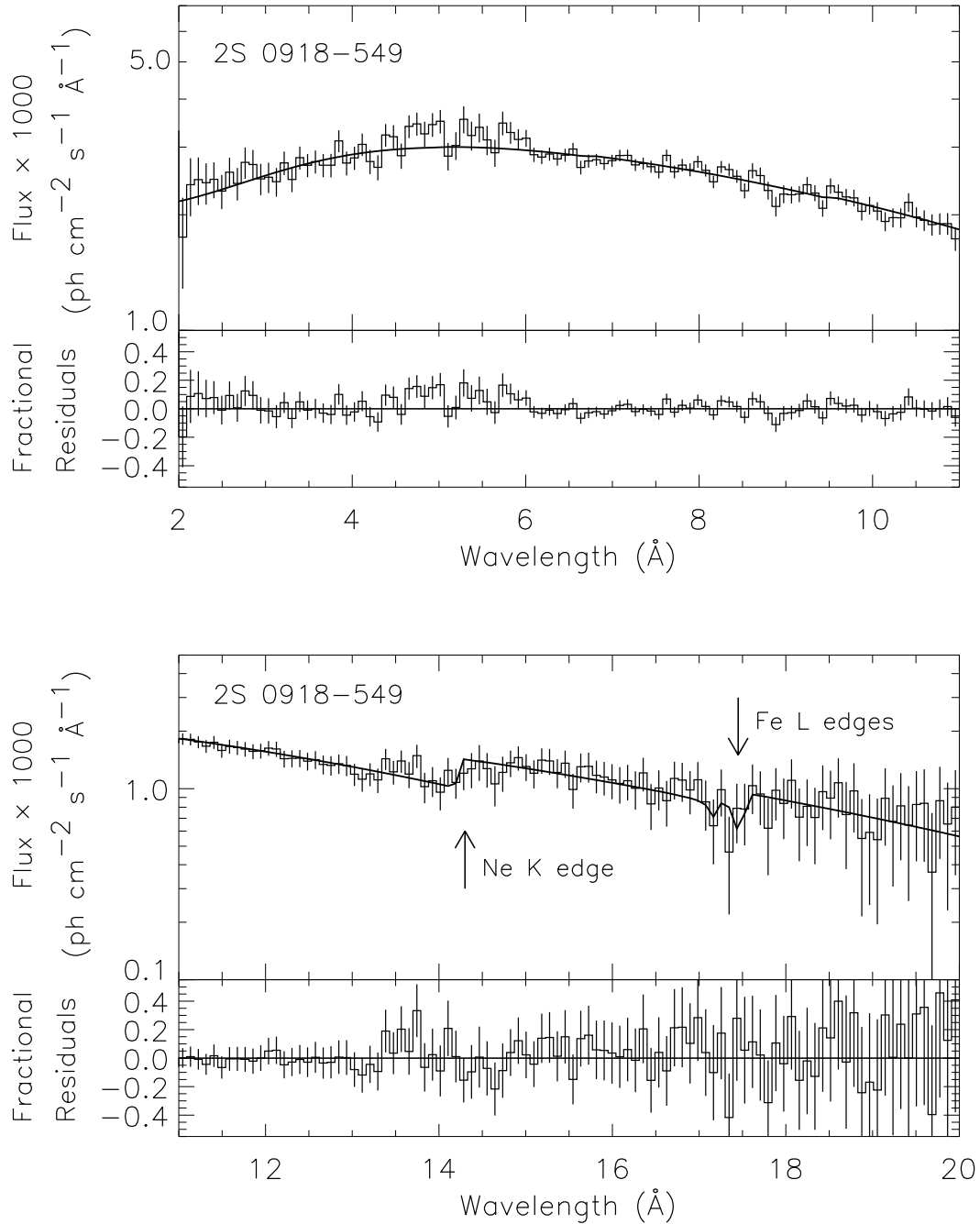


FIG. 2.— (upper panels) *Chandra* MEG first order spectrum of 2S 0918–549 with best-fit power-law + blackbody model including the O, Fe, and Ne edge models. For clarity, the data is binned to 0.09 Å. (lower panels) Fractional residuals ([data–model]/model) of the MEG first order spectral fit shown above. There are no features detected which are consistent with narrow emission or absorption lines. The arrows mark the Ne-K and Fe-L absorption edges at 14.3 and 17.5 Å respectively.

abundances. These results are summarized in Table 2. The atomic cross-sections of Verner et al. (1993) were used for O and Ne, while the Fe-L cross-section was taken from Kortright & Kim (2000). We use both the solar abundances of Morrison & McCammon (1983), as well as the ISM abundances given by Wilms, Allen, & McCray (2000) to calculate equivalent hydrogen column densities. We include the Morrison & McCammon (1983) abundances in order to compare with previous results, but prefer the ISM abundances of Wilms et al. (2000) which are more consistent with recent ISM abundance measurements in the optical and ultraviolet (UV). As can be seen, the equiva-

lent hydrogen column implied by the Ne edge is more than three times that calculated from the O edge. We find a Ne/O number ratio of 0.7 ± 0.3 , compared to the ISM ratio of 0.18. The estimated instrumental C absorption at the time of this observation would account for a C/H ratio of $(1.27 \pm 0.08) \times$ the ISM value (H. L. Marshall, private communication), which is less than the measured C/H ratio of $(5.5 \pm 1.3) \times$ the ISM value. This suggests that there may be C absorption intrinsic to the source, similar to Ne. The measured Fe column is $(13 \pm 7) \times 10^{16} \text{ cm}^{-2}$ and is roughly consistent with interstellar absorption.

The large Ne/O ratio measured for 2S 0918–549 is similar to

TABLE 1
 SPECTRAL FITS^a

Model ^c	Absorption		Power-law		Blackbody		Absorption Line		
	N_{H} (10^{21} cm^{-2})	Carbon Abundance ^b	Γ	A_1^d	kT (keV)	$R_{\text{km}}^2/d_{\text{kpc}}^2$	λ_L (Å)	Flux ^e	χ^2/dof
2S 0918–549									
phabs × (PL+BB)	1.8 ± 0.4	...	1.92 ± 0.14	2.4 ± 0.5	0.54 ± 0.03	0.35 ± 0.12	222/395
vphabs × (PL+BB)	1.8(fixed)	5.5 ± 1.3	2.12 ± 0.09	3.3 ± 0.3	0.57 ± 0.03	0.20 ± 0.08	718/1695
4U 1543–624									
phabs × (PL+BB)	1.34 ± 0.11	...	1.41 ± 0.04	10.7 ± 0.6	0.559 ± 0.017	1.14 ± 0.17	2623/658
vphabs × (PL+BB)	1.34(fixed)	9.3 ± 0.9	1.67 ± 0.04	16.9 ± 0.6	0.52 ± 0.08	0.33 ± 0.25	23.514 ± 0.015	4.6 ⁺³⁸ _{-1.6}	3658/2565

^aAll errors are quoted at the 90%-confidence level

^bCarbon abundance ratio relative to solar, (C/H)/(C/H)_⊕

^cPL=power law; BB=blackbody; phabs=photoelectric absorption with standard abundances; vphabs=photoelectric absorption with non-standard abundances. When using vphabs, the abundances of O, Fe, and Ne were set to zero, edge models were used to model the absorption of O and Ne, and a table model was used to model the Fe L edge. Only the C abundance was varied with vphabs. The results for the edge models are given in Table 2.

^dPower-law normalization at 1 keV in units of 10^{-2} photons keV⁻¹ cm⁻² s⁻¹

^eGaussian flux measurement in units of 10^{-4} photons cm⁻² s⁻¹

that seen in the ultracompact binary pulsar 4U 1626–67 (Schulz et al. 2001). The X-ray spectrum of 4U 1626–67 also reveals emission lines from O and Ne at 0.6 and 1.0 keV respectively (Angelini et al. 1995; Schulz et al. 2001). The strongest of these lines are the hydrogen-like species O VIII and Ne X, which are resolved into broadened, Doppler-shifted pairs in the *Chandra* spectrum (Schulz et al. 2001). The similarity between the two sources led us to look for the presence of such lines in the *Chandra* spectrum of 2S 0918–549. For single Ne and O lines broadened to 5340 and 7460 km s⁻¹ respectively, the 3σ upper limit on the equivalent width (EW) of these lines is 5 eV and 15 eV. The upper limit on the EWs for both lines are below the measured EWs for 4U 1626–67, although the flux limits are comparable or higher (see, Table 3). The helium-like species Ne IX and O VII, have upper limits similar to their hydrogen-like counterparts. If we assume the lines are narrow (widths on the order of the instrument resolution), the upper limits are reduced by as much as a factor of 4.5. We also looked for the presence of Fe K α emission in the range 6.4–6.7 keV. We place an upper limit of 60 eV on the strength of any narrow Fe emission feature in this range.

3.2. 4U 1543–624

We fit the four (+1 and -1; MEG and HEG) spectra of 4U 1543–624 jointly with an absorbed power-law + blackbody model. The residuals from the continuum fit of 4U 1543–624 show evidence for excess Ne absorption at 15–20 Å (see Figure 3). The absorbed 2–10 keV flux is 7.5×10^{-10} erg cm⁻² s⁻¹, which is consistent with past observations, and the best-fit hydrogen column density is $N_{\text{H}} = (1.34 \pm 0.11) \times 10^{21} \text{ cm}^{-2}$. The reddening to the optical counterpart is estimated at $A_V \lesssim 1.0$ mag (Bradt & McClintock 1983), which implies $N_{\text{H}} \lesssim 1.8 \times 10^{21} \text{ cm}^{-2}$ (Predehl & Schmitt 1995). A study of the optical reddening of stars in the direction of 4U 1543–624 finds an average $E_{B-V} = 0.18 \pm 0.06$ for stars beyond 2 kpc (van Paradijs et al. 1986), implying $N_{\text{H}} = (1.0 \pm 0.3) \times 10^{21} \text{ cm}^{-2}$, consistent

with our X-ray measurement.

To fit the high-resolution spectrum of 4U 1543–624, we used a power-law + blackbody model with the absorption by O, Fe, and Ne fit by edge models as was done for 2S 0918–549. Absorption from all other elements was again accounted for by the vphabs model with the N_{H} fixed to the low-resolution result and the C abundance allowed to vary to allow for an unmodeled instrumental contribution. We also included an absorption line at 23.51 Å due to atomic O absorption. This feature is also seen in the high-resolution spectra of 4U 0614+091 and Cyg X-1 (Paerels et al. 2001; Schulz et al. 2002). The best-fit model results are given in Table 1 and the edge depths in Table 2. We find a Ne/O number ratio of 1.8 ± 0.4 , almost $10 \times$ the ISM value, and a C/H relative abundance of $(9.3 \pm 0.9) \times$ the ISM value. The large C/H ratio is not fully explained by the instrumental absorption, which would have given C/H = $(1.87 \pm 0.13) \times$ the ISM value (H. L. Marshall, private communication). This may imply C absorption local to 4U 1543–624. The measured Fe column is again consistent with interstellar absorption.

As can be seen in Figure 4, no emission lines from O, Ne or Fe are apparent in the spectrum of 4U 1543–624. We determined the upper limits on the EW for the same species of Ne and O found in the *Chandra* spectrum of 4U 1626–67 (Table 3). For single Ne X and O VIII lines broadened to 5340 and 7460 km s⁻¹ respectively, the 3σ upper limits on the EWs of these lines are 3.8 eV and 18 eV. These limits are lower than measured EWs in 4U 1626–67, although the flux limits are greater (see Table 3). For the helium-like species Ne IX and O VII, the upper limits are also less than the measured EWs from 4U 1626–67. If we assume the lines are narrow (widths on the order of the instrument resolution), the upper limits are reduced by as much as a factor of 8. The upper limit on the EW of an Fe K line in the 6.4–7.0 keV range is 24 eV. Our upper limit on the EW is consistent with the EW of 48^{+48}_{-31} eV measured by ASCA (Asai et al. 2000), but is less than the 110^{+90}_{-50} eV EW found in the *EXOSAT* data (Singh et al. 1994).

TABLE 2
PHOTOELECTRIC ABSORPTION EDGE MEASUREMENTS^a

Edge	λ (Å)	Optical depth τ	N_Z (10^{17} cm $^{-2}$)	$N_{H,\text{solar}}^c$ (10^{21} cm $^{-2}$)	$N_{H,\text{ISM}}^d$ (10^{21} cm $^{-2}$)
2S 0918–549					
O K	22.5 ± 1.2	0.8 ± 0.4	14 ± 7	1.9 ± 0.9	2.9 ± 1.4
Fe L III	17.49 ± 0.05^b	...	1.3 ± 0.7	4 ± 2	5 ± 3
Ne K	14.3 ± 0.3	0.36 ± 0.08	10 ± 2	7.2 ± 1.4	12 ± 2
4U 1543–624					
O K	23.13 ± 0.09	0.43 ± 0.08	7.6 ± 1.4	1.03 ± 0.19	1.6 ± 0.3
Fe L III	17.51 ± 0.05^b	...	0.21 ± 0.17	0.6 ± 0.5	0.8 ± 0.6
Ne K	14.32 ± 0.03	0.51 ± 0.03	14.0 ± 0.8	10.1 ± 0.6	16.1 ± 0.9

^aAll errors are quoted at the 90%-confidence level. Atomic cross-sections taken from Verner et al. (1993) for O and Ne, and Kortright & Kim (2000) for Fe-L.

^bWe define the absorption edge energy for Fe as the energy at which the edge structure reaches its minimum value.

^cImplied N_H assuming solar abundances of Morrison & McCammon (1983).

^dImplied N_H assuming ISM abundances of Wilms et al. (2000).

We do make a marginal detection (2.8σ) of an unidentified line-like feature at 14.2 Å. This feature is highly broadened when fit by a single gaussian, FWHM=4000 km s $^{-1}$, with an EW of 14 eV. We consider three possible origins for this feature. First, the feature may be instrumental in origin. The feature is more pronounced in the -1 order spectrum and the shape is different when + and – are compared. In addition, the effective area of the -1 spectrum is dropping at the wavelength of the feature due to a chip gap. Combined, this evidence suggests that the feature may not be astrophysical in origin, but rather an instrumental effect due to the uncertainty of the effective area in chip gaps. Unfortunately, there have been no reports of a similar feature around the Ne edge in other sources. A second possibility is that the feature is an emission line or a radiative recombination continuum (RRC) emission feature. At 14.2 Å, emission from a number of different ionization states of Fe is possible, but we would expect to see multiple features (e.g. as in the spectrum of Cyg X-1; Schulz et al. 2002). The O VIII RRC feature is also consistent with the 14.2 Å position. Again though, the lack of other O VIII emission features, in particular the O VIII emission line at 18.97 Å, makes this possibility less probable. Finally, the feature might be related to the Ne absorption edge. However, this is implausible given that Ne is a noble gas. Unlike other elements, Ne cannot be in molecular forms which might cause structure at the K shell absorption edge. We can not rule out however unanticipated structure in the edge shape. In addition, if the Ne-rich absorbing material has some velocity, we might expect to find a velocity shifted edge structure.

4. DISCUSSION

We have shown that the *Chandra*/HETGS spectra of 2S 0918–549 and 4U 1543–624 are well fit with Ne absorption in excess of the predicted interstellar value. The spectrum of 2S 0918–549 is well fit by an absorbed power-law + blackbody and a best fit Ne/O number ratio of 0.7 ± 0.3 , or $3 \times$ the ISM value. The best fit power-law + blackbody model for the

spectrum of 4U 1543–624 has a Ne/O number ratio of 1.8 ± 0.4 , or $10 \times$ the ISM value. These results confirm our previous work with the *ASCA* low-resolution data (Juett et al. 2001) and compare well with the absorption features in the *Chandra*/HETGS spectrum of the ultracompact binary X-ray pulsar 4U 1626–67 (Schulz et al. 2001). In addition, we see good evidence for excess C absorption in the spectra of both sources.

From the L_x/L_{opt} ratios of 2S 0918–549 and 4U 1543–624, we expect these binaries to have orbital periods $\lesssim 60$ min based on the empirical relationship determined by van Paradijs & McClintock (1994). We searched the *Chandra* lightcurves for orbital modulation, but found no modulations larger than 1–2%. Confirmation of such short orbital periods would place 2S 0918–549 and 4U 1543–624 in the class of ultracompact LMXBs ($P_{\text{orb}} \lesssim 80$ min). Ultracompact binaries require H-depleted or degenerate dwarf companions (Joss et al. 1978; Nelson et al. 1986). Such companions would be expected to have non-standard abundances compared to ISM values. The *Chandra* spectrum of 4U 1626–67 revealed absorption edges of C, O, and Ne which are 5 times larger than would be predicted given the hydrogen column density measured in the UV. For 4U 1626–67, the measured local abundance ratios, if the excess material is assumed to have originated around the binary, are consistent with the expected abundances in the chemically fractionated core of a C-O or O-Ne-Mg WD (Schulz et al. 2001). Based on this result, we previously attributed the excess Ne absorption in 2S 0918–549 and 4U 1543–624 to material local to the sources, and suggested that these systems contained a Ne-rich degenerate donor (Juett et al. 2001). Without the independent estimate of N_H from UV spectra, we are not able to calculate the implied local abundances as was done for 4U 1626–67. However, it is interesting to note that the equivalent hydrogen columns calculated from the O edge for both 2S 0918–549 and 4U 1543–624 are marginally consistent with those predicted from E_{B-V} measurements from the optical. Unfortunately, the larger ISM absorption to 2S 0918–549 and 4U 1543–624, compared to 4U 1626–67, may make it difficult to separate out intrinsic and ISM contributions to the absorption without a precise determination of N_H .

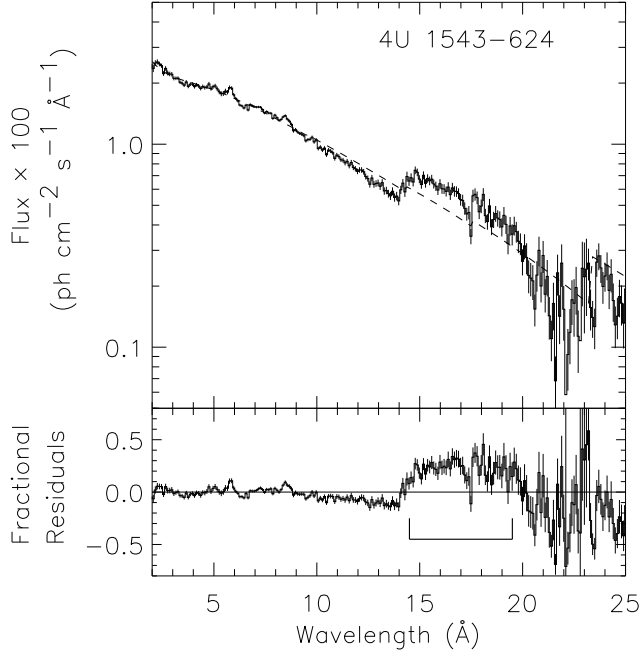


FIG. 3.— (upper panel) Binned MEG first order *Chandra* spectrum of 4U 1543–624 using a standard absorbed power-law + blackbody model. (lower panel) Fractional residuals ([data–model]/model) of the same *Chandra* spectrum and fit. The feature from 15–20 Å is the residual due to the excess absorption from Ne. This feature had originally been attributed to unresolved line emission in low-resolution spectra.

TABLE 3
3 σ UPPER LIMITS ON NE AND O EMISSION LINES

	Ne X	Ne IX	O VIII	O VII
2S 0918–549				
EW (eV)	< 5.0	< 8.8	< 15	< 46
Flux ^a	< 1.8	< 3.9	< 13	< 52
4U 1543–624				
EW (eV)	< 3.8	< 7.2	< 18	< 5.6
Flux ^a	< 74	< 55	< 36	< 19
4U 1626–67 ^b				
EW (eV)	22.5	17.8	24.6	44.4
Flux ^a	2.3	1.8	3.2	3.2

^aFlux in units of 10^{-4} photons $\text{cm}^{-2} \text{s}^{-1}$

^bMeasured equivalent widths and flux of the Ne and O lines for 4U 1626–67 as given by Schulz et al. (2001)

Although we attribute the excess Ne absorption in 2S 0918–549 and 4U 1543–624 to local material in both of the binaries, we should also consider the possibility that the excess Ne is due to enhancements of the ISM along the line of sight. If we assume the uncertainty in both abundances is 0.1 dex (Wilms et al. 2000), then the maximum Ne/O number ratio for ISM abundances is 0.3. Note that our values are 2–6 times larger than even this maximal interstellar Ne/O ratio. In contrast, the best measurement of absorption toward an X-ray binary, the *Chandra* spectral analysis of Cyg X-1, shows columns of O and Ne that are consistent with standard ISM abundances (Schulz et al. 2002). While unusual abundances may occur

along some ISM sight lines, it is unlikely that the sight lines toward five LMXBs (Juett et al. 2001; Schulz et al. 2001) would have the same Ne enhancement. Therefore, we still favor the interpretation that the absorbing material is local to the binaries.

If we assume the absorbing material is due to a wind-like outflow from the companion or the accretion disk, we can estimate the size of the absorbing region. For spherically symmetric mass loss at a constant rate, the number density of species Z as a function of radius is given by

$$n = \frac{\rho_Z}{A_Z m_p} = \frac{\dot{M}_Z}{4\pi v r^2 A_Z m_p}, \quad (2)$$

where ρ_Z is the mass density, A_Z is the atomic number of the species, m_p is the proton mass, \dot{M}_Z is the mass-loss rate, and v is the speed of the outflow. By integrating along the line of sight, we can determine the radius at which the outflow originates in order to provide the required column density N_Z . We find

$$R \simeq 4 \times 10^{10} \text{ cm} \left(\frac{\dot{M}_Z}{10^{-11} M_{\odot} \text{ yr}^{-1}} \right) \left(\frac{v}{10^3 \text{ km s}^{-1}} \right)^{-1} \times \left(\frac{N_Z}{5 \times 10^{17} \text{ cm}^{-2}} \right)^{-1} \left(\frac{A_Z}{20} \right)^{-1}, \quad (3)$$

where we have scaled the equation to parameter values appropriate to the systems under consideration. Not surprisingly, the absorbing region is consistent with the size of an ultracompact binary system. Thus we see that a small mass outflow ($\approx 10\%$ of the accretion rate onto the NS) can provide enough material to account for the measured intrinsic absorption.

Analysis of the *Chandra* spectra of 2S 0918–549 and 4U 1543–624 found no Ne or O lines like those seen in 4U 1626–67. The absence of strong lines in the spectra of 2S 0918–549 and 4U 1543–624 demonstrates that their circumbinary environments are different compared to 4U 1626–67. One possible reason for this difference may be that 4U 1626–67 is a pulsar with $B = 3 \times 10^{12}$ G (Orlandini et al. 1998), while 2S 0918–549 and 4U 1543–624 are likely to have weak magnetic fields ($\sim 10^8$ G). This undoubtedly results in a substantial difference in the accretion flow geometry. There is evidence for a weak line-like feature in the spectrum of 4U 1543–624 at 14.2 Å. The source of the feature is not easily identifiable, but is most likely a combination of instrumental effects and astrophysical emission and/or absorption features.

A recent *RXTE* observation of 2S 0918–549 found the first thermonuclear X-ray burst from this source (Jonker et al. 2001). The burst was short, with an e -folding time of 8.95 ± 0.05 s. If the companion has a large C abundance, we might expect to see a much longer burst (≈ 1 hr), like the “superbursts” seen in some LMXBs, which have been attributed to thermonuclear burning of C on neutron star surfaces (Cornelisse et al. 2000; Cumming & Bildsten 2001; Strohmayer & Brown 2001). The properties of the X-ray burst from 2S 0918–549 may indicate that the donor cannot be a C–O dwarf as suggested for 4U 1626–67. In this case, another mechanism for Ne enhancement is needed. On the other hand, it may still be possible for a carbon accretor to show short X-ray bursts. The heavy elements (C, O, and Ne) may undergo spallation during accretion, leaving He and H nuclei which could then undergo unstable thermonuclear burning in the usual way (Bildsten, Salpeter, & Wasserman 1992).

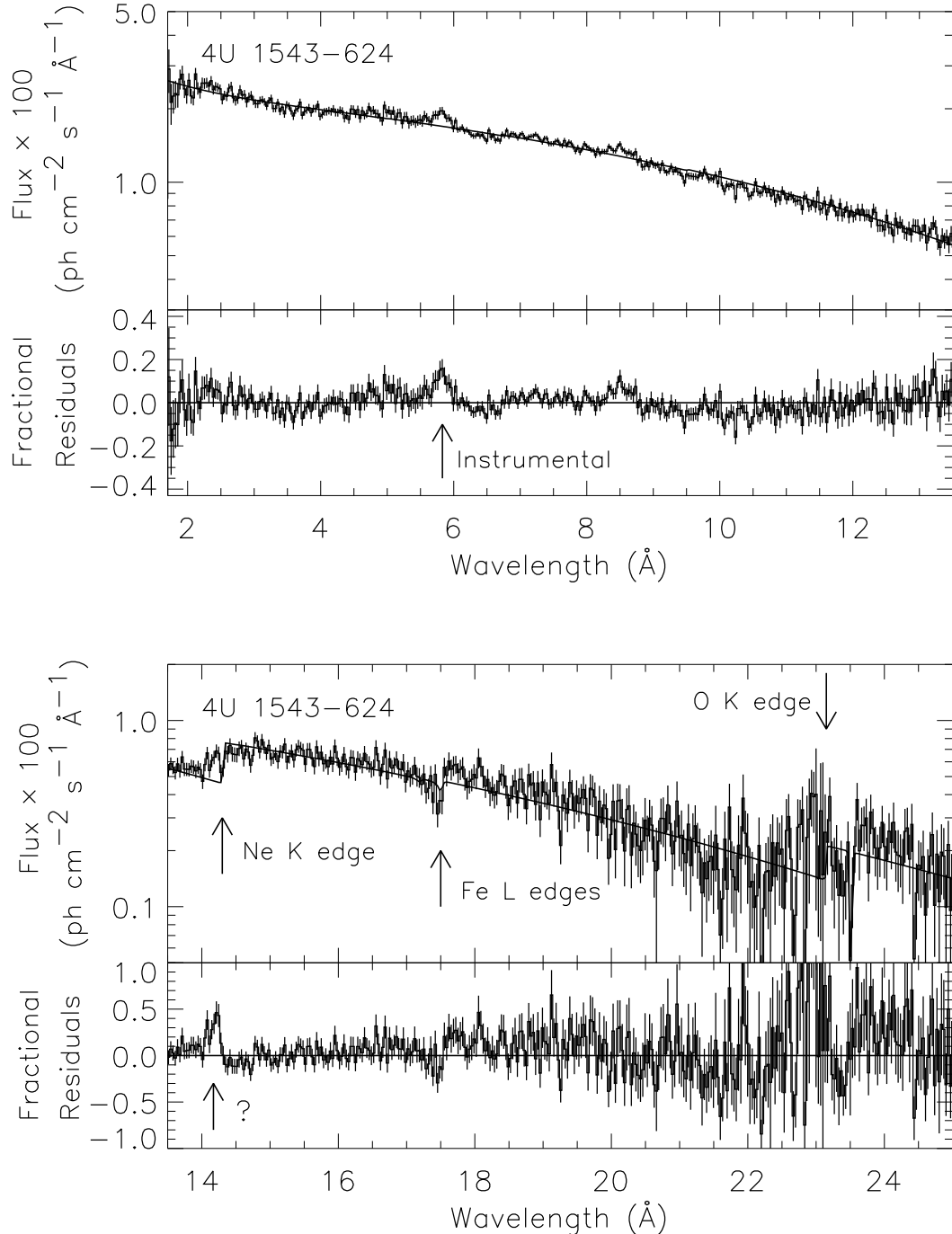


FIG. 4.— (upper panels) *Chandra* MEG first order spectrum of 4U 1543–624 with best-fit model including O, Fe, and Ne edges. (lower panels) Fractional residuals ([data–model]/model) of the MEG first order spectral fit shown above. We have used arrows to identify interesting features in the spectrum, including the Ne, Fe, and O absorption edges. There is a marginal detection (2.8σ) of an emission feature at 14.2 Å of unknown origin. The feature at 5.8 Å is a known instrumental feature due to the effect of pileup on the spectrum around the Ir M instrumental edge at 5.98 Å.

Spallation reactions would produce γ -ray emission lines at 4.4 and 6.1 MeV. Unfortunately, the strength of these lines as calculated by Bildsten et al. (1992) is below current observational detection limits.

We are grateful to the HETGS instrument team at MIT for their help and advice in analyzing these data. We especially thank John Davis for assistance in analyzing piled-up grating

data, John Houck for his help with and modifications of ISIS, and Herman Marshall for information on the ACIS calibration status and the appropriate QE correction table. We also acknowledge useful discussions with Lars Bildsten, Eric Kuulkers, Jon Miller, Mike Muno, Eric Pfahl, Dimitrios Psaltis, and Norbert Schulz. This work was supported in part by NASA under contracts NAS8-38249 and NAS8-01129 and grant NAG5-9184.

REFERENCES

Angelini, L., White, N. E., Nagase, F., Kallman, T. R., Yoshida, A., Takeshima, T., Becker, C., & Paerels, F. 1995, *ApJ*, 449, L41

Asai, K., Dotani, T., Nagase, F., Mitsuda, K. 2000, *ApJS*, 131, 571

Arnaud, K. A. 1996, in *Astronomical Data Analysis Software and Systems V*, ed. G. Jacoby & J. Barnes (San Francisco: ASP Conf. Ser. 101), 17

Bildsten, L., Salpeter, E. E., & Wasserman, I. 1992, *ApJ*, 384, 143

Bradt, H. V. D. & McClintock, J. E. 1983, *ARA&A*, 21, 13

Chevalier, C. & Illovaisky, S. A. 1987, *A&A*, 172, 167

Christian, D. J., & Swank, J. H. 1997, *ApJS*, 109, 177

Christian, D. J., White, N. E., & Swank, J. H. 1994, *ApJ*, 422, 791

Cornelisse, R., Heise, J., Kuulkers, E., Verbunt, F., & in't Zand, J. J. M. 2000, *ApJ*, 357, L21

Cumming, A. & Bildsten, L. 2001, *ApJ*, 559, L127

Davis, J. E. 2001a, *ApJ*, 548, 1010

———. 2001b, *ApJ*, 562, 575

Forman, W. et al. 1978, *ApJS*, 38, 357

Galloway, D. K., Morgan, E. H., Remillard, R. A., & Chakrabarty, D. 2002, *IAU Circ.* 7900

Homan, J. & van der Klis, M. 2000, *ApJ*, 539, 847

Homer, L., Charles, P. A., Naylor, T., van Paradijs, J., Aurère, M., & Koch-Miramond, L. 1996, *MNRAS*, 282, L37

Houck, J. C., & DeNicola, L. A. 2000, *ASP Conf. Ser.*, Vol 216, 591

Jonker, P. G. et al. 2001, *ApJ*, 553, 335

Joss, P. C., Avni, Y., & Rappaport, S. 1978, *ApJ*, 221, 645

Juett, A. M., Psaltis, D., & Chakrabarty, D. 2001, *ApJ*, 560, L59

Kortright, J. B., & Kim, S.-K. 2000, *Phys. Rev. B*, 62, 12216

Markwardt, C. B. & Swank, J. H. 2002, *IAU Circ.*, 7870

McClintock, J., Canizares, C., Hiltner, W. A., & Petro, L. 1978, *IAU Circ.*, 3251

Middleditch, J., Mason, K. O., Nelson, J. E., & White, N. E. 1981, *ApJ*, 244, 1001

Morrison, R. & McCammon, D. 1983, *ApJ*, 278, 1082

Muno, M. P., Remillard, R. A., & Chakrabarty, D. 2002, *ApJ*, 568, L35

Nelson, L. A., Rappaport, S. A., & Joss, P. C. 1986, *ApJ*, 304, 231

Orlandini, M., et al. 1998, *ApJ*, 500, L163

Paczynski, B., & Sienkiewicz, R. 1981, *ApJ*, 248, L27

Paerels, F., et al. 2001, *ApJ*, 546, 338

Predahl, P. & Schmitt, J. H. M. 1995, *A&A*, 293, 889

Schulz, N. S. 1999, *ApJ*, 511, 304

Schulz, N. S., Chakrabarty, D., Marshall, H. L., Canizares, C. R., Lee, J. C., & Houck, J. 2001, *ApJ*, 563, 941

Schulz, N. S., Cui, W., Canizares, C. R., Marshall, H. L., Lee, J. C., Miller, J. M., & Lewin, W. H. G. 2002, *ApJ*, 565, 1141

Singh, K. P., Apparao, K. M. V., Kraft, R. P. 1994, *ApJ*, 421, 753

Smale, A. P., & Lochner, J. C. 1992, *ApJ*, 395, 582

Stella, L., Priedhorsky, W., & White, N. E. 1987, *ApJ*, 312, L17

Strohmayer, T. E. & Brown, E. F. 2002, *ApJ*, 566, 1045

van Paradijs, J., & McClintock, J. E. 1994, *A&A*, 290, 133

van Paradijs, J., van Amerongen, S., Damen, E., & van der Woerd, H. 1986, *A&AS*, 63, 71

Verner, D. A., Yakovlev, D. G., Band, I. M., & Trzhaskovskaya, M. B. 1993, *Atomic Data & Nucl. Data Tables*, 55, 233

Walter, F. M., et al. 1982, *ApJ*, 253, L67

Warner, B. 1995, *Ap&SS*, 225, 249

Warwick, R. S. et al. 1981, *MNRAS*, 197, 865

Weisskopf, M. C., Brinkman, B., Canizares, C., Garmire, G., Murray, S., & van Speybroeck, L. P. 2002, *PASP*, 114, 1

White, N. E., Kallman, T. R., & Angelini, L. 1997, in *X-Ray Imaging and Spectroscopy of Cosmic Hot Plasmas*, ed. F. Makino & K. Mitsuda (Tokyo: Universal Academy Press), 411

White, N. E., & Swank, J. H. 1982, *ApJ*, 253 L61

Wilms, J., Allen, A., & McCray, R. 2000, *ApJ*, 542, 914